J. Fluid Mech. (2011), *vol.* 681, *pp.* 311–339. © Cambridge University Press 2011
doi:10.1017/jfm.2011.200

Bend theory of river meanders with spatial width variations

ROSSELLA LUCHI†, GUIDO ZOLEZZI‡ AND MARCO TUBINO

Department of Civil and Environmental Engineering, University of Trento, via Mesiano 77, 38122 Italy

(Received 22 August 2010; revised 4 April 2011; accepted 28 April 2011; first published online 20 June 2011)

The present work revisits the classical, uniform-width bend theory with the aim to understand whether and how spatial width oscillations can affect the process of linear bend stability that initiates meander planform evolution. Although longitudinal oscillations of channel width are common along many meandering streams, little investigation of their properties and dynamic effects has been pursued so far. The theory therefore accounts for width variations as a geometrical forcing in a depth-averaged model of meander morphodynamics by assuming the potential interaction with the classical curvature forcing effect. A first quantification of width variations is made by referring to a freely evolving meandering river, which shows that the dimensionless amplitude of width variations is a 'small' parameter with comparable magnitude to that of curvature variations, thus suggesting the use of a two-parameter perturbation expansion. Moreover, it is reasonable to assume that channel width oscillates in space with a double frequency relative to curvature, which implies that one nonlinear interaction between the two forcing effects is enough to reproduce the effect of spatial width variations on the process of bend stability. Overall, width variations consistently promote the instability of shorter bends with respect to meanders with uniform width: on average, this predicted tendency is supported by analysis of field data referring to hundreds of natural meander bends. The effect on meander wavelength selection depends on the location of the widest section relative to the bend apex. Under typical formative conditions of gravel-bed rivers, with large-enough channel aspect ratios, two distinct most unstable longitudinal modes develop. Such behaviour is absent when the width is uniform, and suggests a mechanistic interpretation for the reach-scale occurrence of chute cutoffs that can be observed more frequently in wider-at-bends than in equiwidth meandering channels.

Key words: river dynamics, sediment transport

1. Introduction

Nearly three decades ago, the first bend theory of meandering rivers was proposed (Hasegawa 1977; Ikeda, Parker & Sawai 1981) to explain the origin of meanders. The idea behind the bend theory is to investigate the stability of sinusoidal, small-amplitude planform deformations with respect to a straight channel configuration, on

† Present address: Department of Civil, Environmental and Architectural Engineering, University of Genova, via Montallegro 1, 16145 Italy
‡ Email address for correspondence: guido.zolezzi@ing.unitn.it

https://doi.org/10.1017/jfm.2011.200 Published online by Cambridge University Press

the basis of a model relating channel migration with the flow perturbation induced by the weakly meandering planform.

Physically speaking, the presence of a longitudinally-variable channel curvature gives rise to stationary point bars and to a related laterally-asymmetrical longitudinal flow pattern, whereby deeper pools often correspond to faster flow. This creates an excess longitudinal velocity at one bank with respect to the other, which may favour or inhibit meander growth and migration depending on its spatial lag with respect to the curvature distribution.

The first version of the bend theory was based on a very simplified mathematical treatment of the problem of meander morphodynamics, through a linearization of the equations governing flow dynamics and the evolution of the planform geometry. The bend theory has successively been: (i) extended to account for finite-amplitude planform perturbations (Parker, Sawai & Ikeda 1982), (ii) unified with the bar theory (Blondeaux & Seminara 1985) for the formation of migrating free bars in straight (Colombini, Seminara & Tubino 1987) and weakly meandering channels (Tubino & Seminara 1990) and (iii) further extended to study the effect of flow nonlinearities (Seminara & Tubino 1992; Bolla Pittaluga, Nobile & Seminara 2009). It has been receiving field validation in different contexts (e.g. Luchi *et al.* 2007). The development of the bend theory has allowed decisive advances in understanding meander dynamics. Among these, it has enabled the successful prediction of the characteristic spatial scales of developing meanders (Edwards & Smith 2002; Frascati & Lanzoni 2009), the geometric and hydraulic conditions under which a meander can grow and migrate reproducing typical meander loop shapes (Parker, Diplas & Akiyama 1983; Seminara *et al.* 2001; Zolezzi, Luchi & Tubino 2009*b*), and the development of the long-term meander and floodplain dynamics through simulation models (Howard 1992; Sun *et al.* 1996). More recently, deeper investigations based on the bend theory have opened new perspectives on meander dynamics in relationship with the nature of meander instability (Lanzoni & Seminara 2006) and the possible existence of chaotic behaviours (Stolum 1996; Frascati & Lanzoni 2010).

Analogous theories have been proposed more recently to study the river planform stability with respect to a different non-uniform alignment, namely that resulting from spatial oscillations of channel width. The planform stability has been investigated at linear level of a straight channel with regular, longitudinal width variations by Repetto, Tubino & Paola (2002). A bank stability analysis has been implemented in order to analyse the conditions under which the perturbed flow, associated with the central bar pattern induced by periodic width variations, may tend to damp or enhance the given spatial perturbation of channel width. The study of Repetto *et al.* (2002) also aimed to detect the most probable conditions for the onset of channel bifurcations, which may eventually result from sufficiently-intense longitudinal sequences of widening–narrowing.

While spatial variations of channel width have been primarily related to the dynamics of braided rivers, a relatively small number of field studies clearly indicate the potential dynamic relevance of width variations in the case of meandering rivers. Brice (1975) has proposed a form-based classification of river meandering patterns, which has been further refined under NCHRP Project 24-16 resulting in nine different typologies. Five of these typologies include more or less pronounced and regular oscillations of channel width. For some of these meandering styles, the longitudinal variations of channel width can be systematically correlated with the spatial distribution of channel curvature, either peaking at bend apexes for 'wider-at-bends' meanders or displaying some lag relative to curvature. Some other

https://doi.org/10.1017/jfm.2011.200 Published online by Cambridge University Press

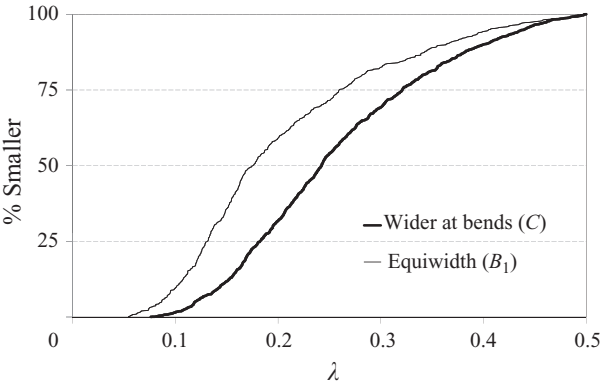


FIGURE 1. Wavenumber distribution of the river bends belonging to class C ('wider at bends') and class B_1 ('equiwidth channel') extracted from the dataset of Lagasse *et al.* (2004).

typologies indicate instead a more irregular width distribution along meander loops. Of particular relevance for the present work is the observation that the degree of width variability along the course of the stream seems to be related with the degree of morphological activity. The analysis of Brice (1982), recently repeated on the larger dataset of Lagasse *et al.* (2004), indicates that wider-at-bends channels display stronger migration rates with respect to equal-width streams.

An even more interesting observation emerges when analysing the differences in meander bend wavelengths between the different types of meandering rivers present in the large dataset of Lagasse *et al.* (2004), based on Brice (1975)'s meander bend dataset. Let λ denote the dimensionless meander wavenumber

$$\lambda = \frac{\pi W^*}{L^*}, \tag{1.1}$$

with W^* and L^* reach-averaged channel width and meander wavelength, respectively. Computing the wavenumber λ for the bends belonging to the 'wider-at-bends' and the 'equiwidth' meander typologies (classes C and B_1, respectively) results in the two distributions of figure 1. It appears that equiwidth meander bends (class B_1) tend to be longer than wider-at-bend meanders (class C). The mean wavenumber values are 0.21 for class B_1 and 0.26 for class C, and their difference is significant with more than 99% probability. On average, this indicates that, when channel width varies in space, meander bends tend to be shorter with respect to meandering rivers with uniform width.

But why should this happen? A possible explanation for the observed differences in meander wavelength and in the degree of morphological activity can be investigated by looking at the feedbacks between flow and bed dynamics in meanders with spatial width variations. Relatively few field observations on the topic are available at present. Longitudinal width variations are often associated with flow deflection around mid-channel bars, as a result of complex feedbacks between river planform and bedform (Luchi, Zolezzi & Tubino 2010*b*). The field observations of Knighton (1972) and Hooke (1986) have described how local widening and the dynamics of associated central bars can significantly contribute to the planform evolution of the most active bends, characterized by high channel mobility and rapid bank erosion. A recurrent sequence of processes has been shown to start with local bend widening, followed by mid-channel bar growth and eventual attachment to the inner bank. This promotes bend growth due to the progressive abandonment of the inner of the two branches

https://doi.org/10.1017/jfm.2011.200 Published online by Cambridge University Press

that previously diverged around the bar (Hooke 1986). When the opposite behaviour applies, the flow concentrates into the inner channel and reproduces a dynamics that can be viewed as analogous to the process of chute cutoff that occurs across the braid bars of braided rivers (Ferguson *et al.* 1992). Such 'bar chute cutoff' differs from floodplain chute cutoffs that reduce sinuosity in meandering rivers through newly cut channels across the floodplain (Constantine, McLean & Dunne 2010). Although the dynamics of both types of chute cutoff is still far from being understood, it can be useful to notice that both field and experimental evidence suggests the close association between the simultaneous presence of spatial width and curvature oscillations and the occurrence of chute cutoffs. Chute cutoffs are almost exclusively associated with meanders that are 'wider-at-bends' in Lagasse *et al.* (2004)'s classification (type *D*) and are a major process governing the morphodynamics of individual branches in braided streams, where the bed and banks evolve at comparable timescales (Bertoldi & Tubino 2005).

All the above observations suggest that spatial width variations can dynamically affect the process of meander development, although a mechanistic understanding of this morphodynamic process is lacking at present. The aim of the present work is to investigate theoretically the coupled dynamics of river planform characterized by the presence of both curvature and width variations as a first step in this direction. We aim to understand on a theoretical basis under which conditions spatial width oscillations can play a relevant role in the dynamics of single-thread meandering channels, and what effect can be expected in terms of meander wavelength selection. The present approach introduces a relatively new perspective on meandering river dynamics. Most existing models for meandering planform evolution indeed assume that the width is constant (Camporeale *et al.* 2007); only few numerical models allow the width to vary in space and time by accounting for the sediment balance resulting from a coupled bed-banks evolution (Darby, Alabyan & Van de Wiel 2002; Yang & Shimizu 2005; Rüther & Olsen 2007; Parker *et al.* 2011). However, none of these models explicitly focus on the role of spatial width variations on meander development.

With this aim, we revisit the classical approach to bend stability (Ikeda *et al.* 1981), by accounting for the presence of both spatial curvature and width variations. The model is based on a depth-averaged formulation of the morphodynamics of a meandering river with spatially variable width, and is solved by means of a perturbation approach. This allows us to identify the hydraulic conditions and planform geometries for which spatial width oscillations can enhance or damp the growth of regular meander sequences.

The paper is organized as follows. The classical approach of bend stability is reviewed in the next section, which points out the key novel features associated with the presence of width variations. Moreover, we provide a first quantification of the typical orders of magnitude of the amplitude and frequency of spatial width variations in meandering rivers. Section 3 presents the formulation of the mathematical model which is solved by means of a two-parameters perturbation approach described in § 4. Results are illustrated in § 5. Section 6 aims to place the present bend theory in a broader perspective by relating the key outcomes with existing field, experimental and theoretical work. Section 7 concludes the paper.

2. Bend stability: physical processes and key assumptions

To revisit the process of bend stability for channels with spatially variable width, it is useful to first review the key concepts on which the classical bend theory for

https://doi.org/10.1017/jfm.2011.200 Published online by Cambridge University Press

equiwidth meanders is built, and, after doing that, to conceptually formulate how the dynamic effect of width variations can be incorporated. Moreover, since the geometry of spatial width variations in meanders has not been quantified previously, a first attempt is made to quantify the order of magnitude of their amplitude, frequency and longitudinal position along a freely evolving meandering river.

2.1. *Bend theory*

The classical bend theory, originally developed by Ikeda *et al.* (1981) and, independently, also by Hasegawa (1977), is based on relating channel migration with reach-averaged bankfull hydraulic conditions. Net channel migration in natural rivers results from the lateral shift of both channel banks, subject to different rates of erosion and accretion that are variable in space and intermittent in time. The migration law traditionally employed by bend theories (e.g. Hasegawa 1989) is based on two key simplifying hypotheses. First, it is assumed that the bank migration process can be represented as a continuous, rather than an intermittent process, at least for the long time scales of meander planform evolution. Moreover, at each cross-section, the two opposite banks are assumed to shift laterally at the same rate, so as to keep channel width constant in time and space.

The rate of net channel shift therefore coincides with the migration rate of both the eroding and the accreting bank. The actual process of bank erosion mainly results from coupled fluvial erosion and mass wasting, which depends on a complex interaction between physical–biological effects including pore water pressures, characteristics of streamflow variability, bank cohesion and riparian vegetation properties (e.g. Rinaldi & Darby 2007). The bank erosion rate is typically assumed to be driven by an excess near-bank shear stress relative to a reach-averaged value. Conversely, the bank accretion rate is related with a defect of flow speed at the inner bank, and is not treated explicitly because very little is presently known on the actual mechanisms that control bank advance. The migration law employed in classical bend theories therefore reads, in dimensionless form:

$$\zeta(s) = E\,[u_{lb}(s) - u_{rb}(s)], \tag{2.1}$$

where $\zeta(s)$ denotes the net rate of channel shift, s is the streamwise coordinate, u_{lb} and u_{rb} represent near-bank (left and right, respectively) excess longitudinal velocity and E is an empirical erosion coefficient accounting for complex bank characteristics (Hasegawa 1989). Despite its strong simplification, the suitability of the above relation has received some support (Pizzuto & Meckelnburg 1989) from field observations on rivers with fairly uniform cohesive banks.

The excess near-bank longitudinal velocity is typically obtained from the solution of the depth-averaged differential problem for steady, non-uniform flow and sediment transport in a constant-width meandering channel with a cohesionless bed. This is usually achieved by linearizing the governing equations by assuming that flow and bed topography deformation due to the meandering planform can be viewed as small-amplitude deviations from a reference basic state, consisting of a uniform flow over a flat bed in a straight channel that carries the same bankfull discharge and has the same slope, sediment size and reach-averaged bankfull width. This assumption holds provided the channel geometry (i.e. the axis curvature in this case) is slowly varying in space, as is indeed typical for many natural meander loops.

Without losing generality, bend theories have often been developed referring to an idealized meandering planform consisting of an indefinite sequence of sine-generated (Langbein & Leopold 1964) meander bends of constant width. This

https://doi.org/10.1017/jfm.2011.200 Published online by Cambridge University Press

assumption has been considered as an effective, although approximate, representation of natural conditions, at least when focussing on an understanding of the underlying physical processes. In this case, the curvature of the channel axis takes the following dimensionless form:

$$\nu\mathscr{C}(s) = \nu\,[\exp(\mathrm{i}\lambda s) + \exp(-\mathrm{i}\lambda s)] = \nu\,[e_1(s) + \bar{e}_1(s)]; \quad \nu = \frac{W^*}{2R_0^*}, \tag{2.2}$$

where λ is the meander wavenumber already defined in (1.1), and ν quantifies the amplitude of curvature variations. Moreover $\mathscr{C}(s)$ is an $O(1)$ function for which the complex exponential notation has been conveniently employed. A star denotes dimensional quantities and an overbar denotes the conjugate of a complex number. Finally R_0^* is a representative value of the channel radius of curvature, say twice the radius of curvature at the bend apex when the channel axis is described by a sine-generated curve.

The near-bank excess linear velocity perturbation in such meandering configuration has the same spatial frequency of the curvature distribution and its amplitude has the same order of magnitude of ν. The linear solution for the longitudinal velocity, scaled through the reference uniform flow velocity, reads (e.g. Blondeaux & Seminara 1985):

$$U(s,n) = 1 + \nu[U_{10}(n)e_1(s) + \bar{U}_{10}(n)\bar{e}_1(s)], \tag{2.3}$$

where n is the transverse coordinate. The lateral velocity profile $U_{10}(n)$ is antisymmetrical: $U_{10\,(\text{right bank})} = -U_{10\,(\text{left bank})}$. According to (2.1), this therefore gives a net contribution to channel migration rate corresponding to $2\nu E U_{10\,(\text{right bank})}$.

We now conceptually examine the possible dynamic role of channel width variations. The linear solution of Repetto *et al.* (2002) refers to an indefinite sequence of sinusoidal channel width oscillations that can be described in dimensionless form by the following expression:

$$W(s) = 1 + \delta\,[\exp(\mathrm{i}\lambda_w s) + \exp(-\mathrm{i}\lambda_w s)]; \quad \lambda_w = \frac{\pi W_0^*}{L_w^*}; \quad \delta = \frac{W_{max}^* - W_0^*}{2W_0^*}, \tag{2.4}$$

where $W(s)$ denotes the local channel width $W^*(s)$ scaled by the reach-averaged value W_0^* and λ_w is the spatial frequency of width variations with dimensional wavelength L_w^*. The relative amplitude of width oscillations is quantified by the parameter δ with W_{max}^* being the maximum value of the channel width in the reach. The corresponding linear flow solution reads (e.g. Repetto *et al.* 2002):

$$U(s,n) = 1 + \delta[U_{01}(n)\,\mathrm{e}_w(s) + \bar{U}_{01}(n)\,\bar{\mathrm{e}}_w(s)], \tag{2.5}$$

where we have set $\mathrm{e}_w(s) = \exp \mathrm{i}\lambda_w s$. Also, in this case, the linear flow perturbation has the same longitudinal frequency of the planform forcing effect, while the lateral flow profile is symmetrical with respect to the channel axis, in association with the lateral symmetry of the central bar pattern associated with width variations: $U_{01\,(\text{right bank})} = U_{01\,(\text{left bank})}$. According to (2.1), this, therefore, does not produce any net effect on lateral channel migration.

The above considerations suggest that a linear morphodynamic solution for meandering channels with spatially variable width does not produce any additional effect with respect to the classical equiwidth linear bend theory. In order to assess possible dynamic effects of width variations on bend stability, and therefore on meander growth, higher-order interactions need to be further explored. A correction to the linear solution (2.3) that can be effective for bend stability, can be obtained

https://doi.org/10.1017/jfm.2011.200 Published online by Cambridge University Press

at whatever order of approximation is able to reproduce an asymmetric transversal perturbation of the velocity U, at the same fundamental frequency λ of the curvature forcing. In terms of a perturbation approach, this requires an expansion of the unknowns in terms of the two 'small' perturbation parameters ν and δ accounting, in principle, for both self and mixed interactions appearing at the second ($\nu\delta$, ν^2, δ^2) and higher orders of approximation. It is easy to show that self second-order interactions (ν^2, δ^2) give rise to laterally symmetrical velocity profiles (see also Seminara & Tubino 1992; Luchi *et al.* 2010*b*), that therefore are not relevant for bend stability. On the contrary, the mixed second-order response $O(\nu\delta)$ takes the following form:

$$U(s,n) \sim \nu\delta\{U_{11}(n)\exp[\mathrm{i}(\lambda \pm \lambda_w)s] + \bar{U}_{11}(n)\exp[-\mathrm{i}(\lambda \pm \lambda_w)s]\}, \tag{2.6}$$

which can reproduce the longitudinal structure of the fundamental (linear) meander solution provided

$$\lambda \pm \lambda_w = \lambda; \quad -\lambda \mp \lambda_w = \lambda, \tag{2.7}$$

which implies

$$\lambda_w = \pm 2\lambda, \tag{2.8}$$

or

$$\lambda_w = 0. \tag{2.9}$$

Planforms characterized by (2.9) represent the limit condition of uniform width, because they correspond to infinitely long (and therefore vanishing) width variations and thus are not meaningful for the present analysis. The positive solution of (2.8), $\lambda_w = 2\lambda$, therefore indicates that spatial width variations can affect the process of bend stability provided their oscillation frequency is twice that of channel curvature, i.e. when a width peak can be found in each adjacent bend, regardless of bend orientation. This represents a key requirement for the development of the present bend stability analysis.

Despite the large number of studies on the geometry of river meanders, however, nearly no quantitative analysis is available to quantify the properties of width variations in natural meandering rivers. A first attempt is therefore needed to substantiate (2.8) and to assess how the perturbation scheme can be correctly developed. This attempt is pursued in the next subsection.

2.2. *Width variations in natural meandering rivers*

Before detecting its variations, channel width itself should be properly defined, which can be pursued using different procedures (Luchi *et al.* 2010*a*). A reasonable working option is to use the free surface width, a hydraulic quantity that not only reflects longitudinal changes in cross-sectional geometry but also of flow stage in the same river reach. Corresponding to point bars near bend apexes indeed, small changes in flow stage may result in relatively large width variations due to the gently sloping lateral bed profile in the inner part of bends. A reference discharge value must therefore be established to compute channel width in meanders. The bend theory of Ikeda *et al.* (1981) and nearly all the successive meander morphodynamic models are based on a continuous representation of the intermittent process of meander evolution, and use a constant discharge representative of formative conditions, for which the bankfull value has been shown to represent a suitable approximation (Hey 1982; Carling 1988).

Having established a working hypothesis to compute channel width, based on bankfull conditions, the following information needs to be quantified to develop a bend stability analysis with spatially variable width: the magnitude and frequency of

https://doi.org/10.1017/jfm.2011.200 Published online by Cambridge University Press

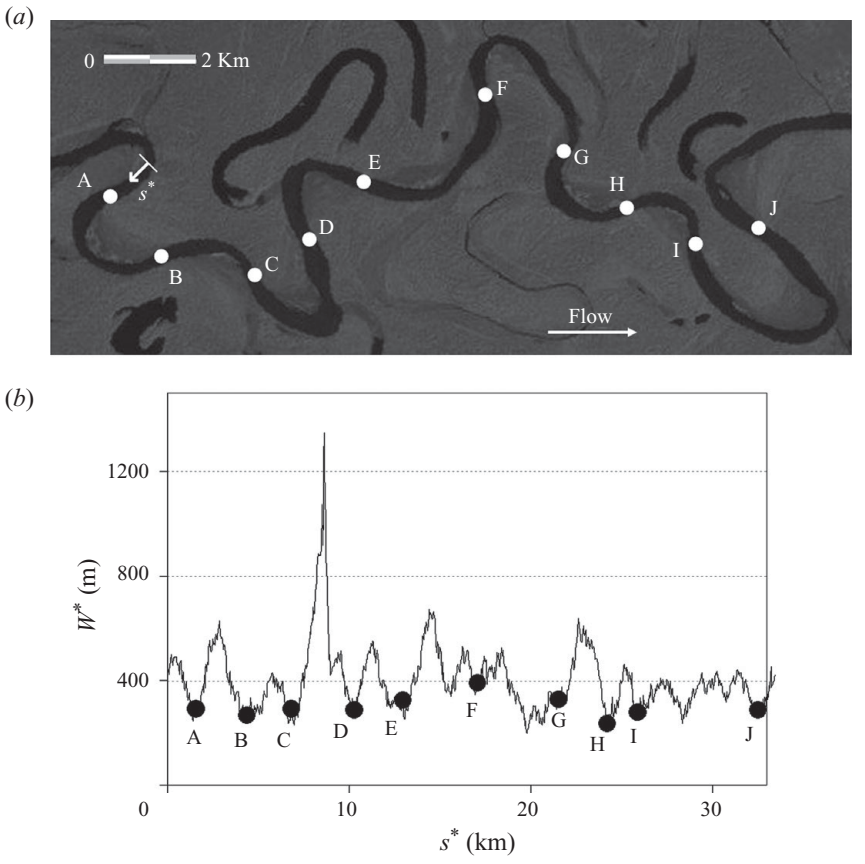


FIGURE 2. (*a*) Satellite images of a reach of the Rio Beni (Bolivian Amazon) in 2000. (*b*) Oscillation of channel width W^* along the same reach. Capital letters (A, ..., J) denote the position of meander inflections.

width oscillations, and their phase lag with respect to the curvature fluctuations. In the absence of a systematic field study on the topic, we have made a first attempt, which, far from being exhaustive, aims to provide at least an order of magnitude estimate for these quantities.

The analysis refers to the Rio Beni, a free meandering river flowing in the Bolivian Amazon. The Beni is a large southern tropical river draining the Andean and sub-Andean ranges and flowing into the Madeira River (Gautier *et al.* 2007). Over a distance of approximately 250 km in the south-western Amazonian lowlands of Bolivia, the Rio Beni develops highly mobile meanders in the floodplain without the input of significant lateral tributaries. Figure 2(*a*) shows a portion of this meandering reach, while the correspondent longitudinal variations of channel width W^* are reported in figure 2(*b*) as a function of the curvilinear arclength s^*. In both images, cross-sections corresponding to meander inflections have been denoted with capital letters (A, ..., J) and by means of full circles that appear white in figure 2(*a*) and black in figure 2(*b*). The reach located between two successive inflection sections is denoted as a 'bend'. The width series has been extracted through a semi-automated procedure based on a supervised classification of the 2000 satellite image covering the reach. First, the channel centreline was extracted using the Matlab® morphological

https://doi.org/10.1017/jfm.2011.200 Published online by Cambridge University Press

Image Processing toolbox and, subsequently, the channel width was computed as the distance between the two banks measured orthogonally to the channel centreline. It is reasonable to assume, as a first approximation, that the bankfull channel is that including both wet and bare sediment areas at the time the image was taken. These areas can also easily be separated from the floodplain vegetation in the classification of the original satellite image.

An inspection of the width series reported in figure 2(*b*) shows that up to seven over the nine bends located between two subsequent inflection sections (A, ..., J) show a common behaviour: channel width peaks once between two successive inflections, which, in turn, coincide with local width minima. Given that one entire meander wavelength is formed by two subsequent bends, this might reveal a tendency of channel width to display two maxima over one meander wavelength. In the case of regular, sine-generated meanders, this would imply:

$$L^* = 2L_w^*, \quad \text{or} \quad \lambda_w = 2\lambda, \tag{2.10}$$

thus supporting the suitability of (2.8) for some natural meandering rivers, at least as a first approximation. Such behaviour is more marked in low-amplitude simple bends where the position of the widest section is well identifiable. The relationship (2.10) is consistent with the observation of Luchi *et al.* (2010*a*) on the River Bollin (UK), a small-scale, gravel-bed meandering river that strongly differs from the Rio Beni, and was already argued, among others, by Parker (1984) and Seminara (2006), although in the absence of direct quantifications.

An analysis of the width series referring to a longer reach of the Rio Beni, including 31 bends, also allows the rough quantification of the amplitude of channel width oscillations and detection of the relative distance between the widest and most curved cross-sections. An average measure of the degree of width variations can be provided by the standard deviation of the spatial width series which is reported in figure 3(*a*), where it has been scaled with the bend-averaged width value for each of the 31 bends extracted from the analysed reach. Few bends have been excluded from the computation, namely those where maximum width and curvature locations along the bend could not be easily identified. These are high-amplitude bends, like that from inflection I to inflection J, and bends tending to have multiple loops behaviour, like that from inflection F to inflection G. Figure 3(*a*) shows that bankfull width oscillations have a dimensionless standard deviation ranging between 0.1 and 0.4, with only very few exceptions. This corresponds to peak width values that can be up to 1.4 times larger than the reach-averaged value, or δ values (2.4) below 0.2.

The quantity $l_{W^*_{max}} - l_{C^*_{max}}$ reported on the vertical axis of figure 3(*b*) represents the position of the widest section relative to the bend apex, defined as the most curved cross-section. It is plotted against the location of the same section relative to the upstream inflection section (the quantity $l_{W^*_{max}} - l_0$ reported on the horizontal axis, see also figure 3*c* for notations). Values have been normalized with the bend length $L^*/2$. Often, the widest section does not coincide with the bend apex, which may be located at variable distances along the meander bend. Only in perfectly sine-generated meander bends is the bend apex indeed located at exactly the half way point between two successive inflections. The widest section in a natural meander bend can both anticipate or follow the bend apex. Figure 3(*b*) provides an order of magnitude of this relative distance, which is less than half the bend length (i.e. one quarter the meander wavelength L^*) for all the bends in the examined reach. Moreover, in 74 % of the analysed bends, the distance between the widest section and the upstream inflection

https://doi.org/10.1017/jfm.2011.200 Published online by Cambridge University Press

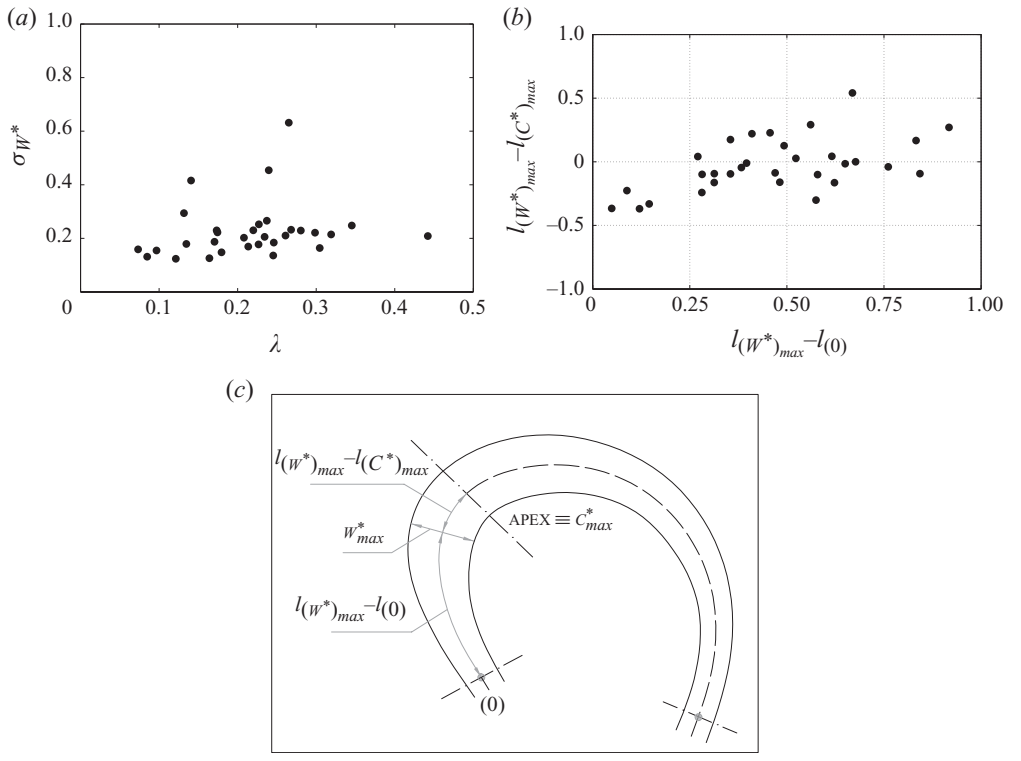


FIGURE 3. Amplitude of width variations and location of the widest section for some bends of the Rio Beni. (*a*) Plot of the dimensionless standard deviation σ_{W^*} of the width series as a function of meander wavenumber λ; (*b*) position of widest section relative to the bend apex ($l_{(W^*)_{max}} - l_{(C^*)_{max}}$) against the location of the same section relative to the upstream inflection section ($l_{W^*_{max}} - l_0$). The dimensionless distances l are measured along the curvilinear coordinate s^* normalized with the bend length ($L^*/2$). (*c*) Sketch of notations employed in (*b*).

ranges between 1/4 and 3/4 of the bend length. Only for a few bends is the maximum of channel width located closer to the meander inflections.

The results of this preliminary analysis allow the formulation of an analytical expression describing the spatial width variations in a sine-generated meander sequence suitable for the present bend stability analysis. We therefore assume that width variations also are periodical in space with a double frequency relative to the fundamental frequency of channel curvature ($\lambda_w = 2\lambda$). Their amplitude δ is a relatively small number $O(10^{-1})$ and their spatial lag with respect to the curvature distribution generally remains less than one quarter of the meander wavelength. It is convenient to use the parameter ω to measure the distance between the widest and the most curved cross-section. It is defined as follows:

$$\omega = -\pi \left(l_{W^*_{max}} - l_{C^*_{max}} \right). \tag{2.11}$$

Regardless of bend orientation, when $\omega = 0$, the channel width peaks at bend apexes, while positive (negative) values of ω correspond to the widest section being located upstream (downstream) the bend apex. The spatial distribution of the dimensionless channel width can therefore be expressed as follows:

$$W(s) = \frac{W^*(s)}{W_0^*} = 1 + \delta[\mathrm{e}^{(2\mathrm{i}(\lambda s + \omega))} + \text{c.c.}]. \tag{2.12}$$

https://doi.org/10.1017/jfm.2011.200 Published online by Cambridge University Press

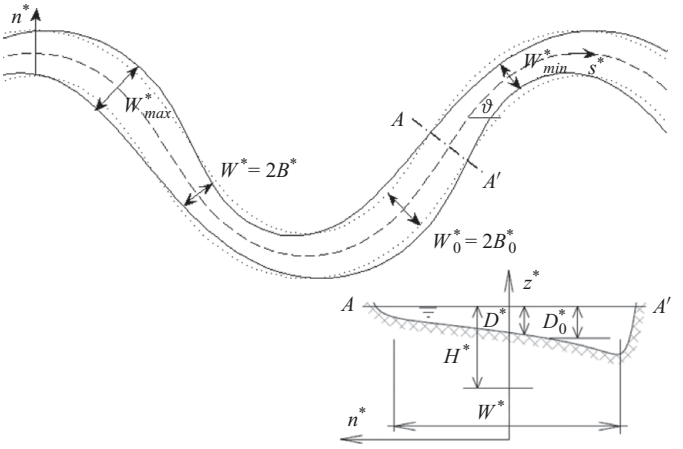


FIGURE 4. Sketch of a meandering channel with spatially variable channel width and notations.

3. Formulation of the model

The study is referred to a meandering channel with spatially variable width W^* (figure 4) with constant longitudinal slope and non-cohesive bed with uniform sediment size d_s^*. We conveniently employ an intrinsic orthogonal curvilinear system of coordinates (s^*, n^*, z^*), which is right-handed with the s^* axis locally downstream directed and the vertical z^* aiming upwards. The shallow water approximation typically holds because meandering occurs at spatial scales of the order of several channel widths. Flow and bed topography can be obtained according to a quasi-steady approximation, which considers that meander planform (channel curvature and width) varies on a much longer time scale with respect to bed and flow deformation. Morphodynamic models at these large spatial scales typically employ a depth-averaged formulation of the Reynolds-averaged Navier–Stokes equations based on appropriate parameterization of secondary flows related to streamline curvature. Secondary flows have vanishing depth average and significantly contribute to channel morphodynamics through the generation of transverse near-bed shear stresses and momentum redistribution. Streamlines are curved both because of channel curvature and spatial width variations, and a suitable parameterization procedure must be employed to retain these dynamic effects.

It is therefore convenient to first introduce the 3D mathematical formulation for a meandering channel with variable width and successively recall the steps of the adopted depth-averaging procedure. Focusing on the central flow region and neglecting sidewall effects, the governing equations are the longitudinal and transverse 3D Reynolds equations and the continuity equations for the fluid and solid phase, the Reynolds equation in the vertical direction simply implying the hydrostatic vertical pressure distribution. They take the following dimensionless form:

$$Nu(u_{,s} - nb_s u_{,n}) + B^{-1} v u_{,n} + w u_{,z} + \nu\, N\mathscr{C} u v = -N(h_{,s} - nb_s h_{,n}) + N\beta\, C_{f0} + \beta \sqrt{C_{f0}}(\nu_T u_{,z})_{,z}, \quad (3.1)$$

$$Nu(v_{,s} - nb_s v_{,n}) + B^{-1} v v_{,n} + w v_{,z} - \nu\, N\mathscr{C} u^2 = -B^{-1} h_{,n} + \beta \sqrt{C_{f0}}(\nu_T v_{,z})_{,z}, \quad (3.2)$$

$$N(u_{,s} - nb_s u_{,n}) + B^{-1} v_{,n} + \nu\, N\mathscr{C} v + w_{,z} = 0, \quad (3.3)$$

https://doi.org/10.1017/jfm.2011.200 Published online by Cambridge University Press

$$N(q_{s,s} - nb_s q_{s,n}) + B^{-1} q_{n,n} + \nu\, N\mathscr{C} q_n = 0, \tag{3.4}$$

where a Boussinesq-type closure (ν_T denoting the eddy viscosity) is used to link turbulent stresses to the turbulence-averaged velocity vector (u, v, w), as is common in many large-scale morphodynamic models. Moreover, h denotes the free surface elevation, D the flow depth and (q_s, q_n) the sediment transport rate per unit width. Variables have been normalized using reach-averaged quantities to achieve more generality and to facilitate comparison of the relative magnitude of different physical effects. The scaling relationships read as follows:

$$(s^*, n^*) = (B_0^* s, B^* n), \tag{3.5}$$

$$(z^*, h^*, D^*) = D_0^* \left(z, F_0^2 h, D\right), \tag{3.6}$$

$$(u^*, v^*, w^*) = U_0^* \left(u, v, \frac{w}{\beta}\right), \tag{3.7}$$

$$(q_s^*, q_n^*) = (q_s, q_n)\sqrt{g \Delta d_s^{*3}}, \tag{3.8}$$

$$(\nu_T^*) = \nu_T(\sqrt{C_{f0}} U_0^* D_0^*). \tag{3.9}$$

Note that a star (*) is used to denote dimensional quantities and the subscript '$_0$' refers to reach-averaged bankfull conditions, taken to coincide with a uniform flow in a straight channel with the same longitudinal slope, flow discharge, uniform sediment size and average channel width. Moreover, the transverse variable n^* has been stretched with the local value of the half channel width $B^*(s^*)$, thus transforming the original domain in the dimensional (s^*, n^*) coordinate system into a rectangle in the (s, n) stretched system. Moreover, Δ denotes the relative submerged sediment density, d_s^* the mean sediment diameter and g the gravitational acceleration. Transverse variable stretching (3.5) implies the following transformation of the spatial derivatives:

$$\frac{\partial}{\partial s^*} \to \frac{1}{B_0^*}\left[\frac{\partial}{\partial s} - nb_s \frac{\partial}{\partial n}\right], \quad \frac{\partial}{\partial n^*} \to \frac{1}{B_0^*}\left[\frac{1}{B(s)}\frac{\partial}{\partial n}\right], \quad b_s = \frac{1}{B(s)}\frac{\partial B}{\partial s}, \tag{3.10}$$

with $B(s) = W^*(s)/(2B_0^*)$ the dimensionless local half channel width. Finally, $N^{-1} = [1 + \nu n B(s)\mathscr{C}(s)]$ is the metric coefficient of the curvilinear coordinate system, $\mathscr{C}(s)$ is the dimensionless channel curvature and F_0 the Froude number of the reference uniform flow. The aspect ratio β, the Shields parameter τ_* and the relative roughness d_s can be used to define the reach-averaged hydraulic conditions. Denoting with C_{f0} the reference dimensionless friction coefficient, they read:

$$\beta = \frac{B_0^*}{D_0^*}, \quad \tau_* = \frac{F_0^2 C_{f0}}{\Delta d_s}, \quad d_s = \frac{d_s^*}{D_0^*}. \tag{3.11}$$

The governing system (3.1, ..., 3.4) is associated with the following boundary conditions:

(i) no slip at the near-bed conventional reference elevation z_0:

$$u = v = w = 0 \qquad (z = F_0^2 h - D + z_0), \tag{3.12}$$

(ii) stress continuity at the free surface:

$$u_{,z} = v_{,z} = 0 \qquad (z = F_0^2 h), \tag{3.13}$$

(iii) impermeable side walls.

Having ignored the role of the side walls on the central flow region, boundary conditions in the lateral domain impose the walls of the channel to be impermeable

https://doi.org/10.1017/jfm.2011.200 Published online by Cambridge University Press

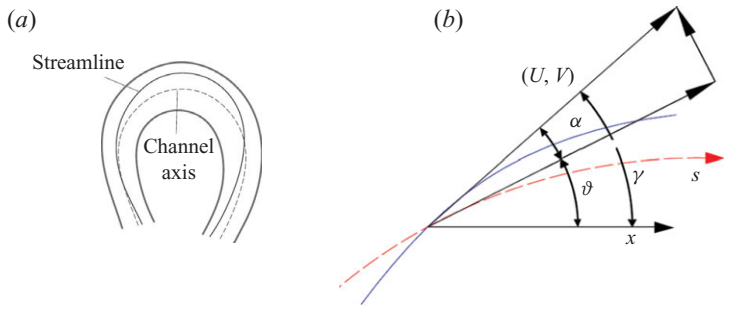


FIGURE 5. (Colour online available at journals.cambridge.org/FLM) (*a*) Qualitative sketch of a streamline and of the channel axis in a meander bend; (*b*) notations employed to denote the angles between the downvalley direction and the local tangents to the channel axis and to the streamline.

both to flow and sediments. Denoting with $\hat{\boldsymbol{n}}_b$ the unit vector normal to the bank lines and with $\boldsymbol{u}$ the velocity vector (u, v, w) and $\boldsymbol{q}$ the sediment transport rate vector (q_s, q_n) yields:

$$\int_D (\boldsymbol{u}\cdot\hat{\boldsymbol{n}}_b)\mathrm{d}z = (\boldsymbol{q}\cdot\hat{\boldsymbol{n}}_b) = 0 \quad (n = \pm 1). \tag{3.14}$$

Note that the differential problem (3.1)–(3.4) correctly reduces to the 3D model for a meander with constant width (e.g. Zolezzi & Seminara 2001) by setting $B^* = B_0^*$. The formulation for a straight channel with variable width (Repetto *et al.* 2002) is analogously recovered by setting $\mathscr{C} = 0$, $N = 1$ and $\nu = 0$. The key feature of the present formulation is its ability to fully describe the morphodynamics of a meandering channel with spatially variable width, including the combination of both planform forcings and their separate effects.

Derivation of suitable depth-averaged morphodynamic models requires appropriate description of the dynamical effects of secondary flows with vanishing depth average, already described by a variety of experimental and theoretical contributions (e.g. among others, Rozovskij 1957; Johannesson & Parker 1989; Seminara & Solari 1998; Blanckaert & de Vriend 2004). Several approaches have been proposed to parameterize their effects into depth-averaged morphodynamic models (Kalkwijk & De Vriend 1980; Seminara & Tubino 1989; Zolezzi & Seminara 2001; Repetto *et al.* 2002). The present depth-averaging procedure follows the classical decomposition of the local transverse velocity v into a 'helical' component v_0 with vanishing depth average, induced by streamline curvature, and a fully 2D component V associated with topographic steering effects (e.g. Kalkwijk & De Vriend 1980). We closely follow the approach of Zolezzi & Seminara (2001) except for replacing the curvature of channel axis with that of depth-averaged streamlines (figure 5*a*) to quantify centrifugal effects. According to (3.1) of Zolezzi & Seminara (2001), the transverse velocity v is therefore written as follows:

$$v = \epsilon\, v_0(s, n, z) + V(s, n)\mathscr{F}_0(z). \tag{3.15}$$

In (3.15), $\mathscr{F}_0(z)$ is the classic vertical logarithmic velocity distribution and ϵ is a typical measure of the streamline curvature, computed as the ratio between B_0^* and a typical value of streamline radius of curvature along the examined reach. In natural rivers, the deviation of depth-averaged streamlines from the channel axis can be considerable and can be due to bed topography deformations or spatially non-uniform planform geometry. Repetto *et al.* (2002) have shown the importance of centrifugally

https://doi.org/10.1017/jfm.2011.200 Published online by Cambridge University Press

induced secondary flows driven by curved streamlines in a straight channel with regular width oscillations, where the curvature of the channel axis vanishes. For this reason, streamline curvature needs to be used instead of channel axis curvature to parameterize secondary flows in morphodynamic models of meanders with spatially variable width.

Referring to figure 5*b*, a suitable expression for the dimensionless streamline curvature $\mathscr{C}_s$ can be obtained. Because transverse variable stretching (3.5) results in several additional terms for the spatial derivatives, for the sake of clarity it is convenient to report the expression of $\mathscr{C}_s$ in the unstretched dimensionless coordinate system $(s, \hat{n}) = (s^*, n^*)/B_0^*$ instead of (s, n):

$$\epsilon \mathscr{C}_s(s, \hat{n}) = -\frac{\partial}{\partial s}\gamma(s, \hat{n}) = -\left[\frac{\partial}{\partial s}\vartheta(s) + \frac{\partial}{\partial s}\alpha(s, \hat{n})\right] = \nu\mathscr{C}(s) - \frac{\partial \alpha(s, \hat{n})}{\partial s}. \tag{3.16}$$

As indicated in figure 5(*b*), in (3.16), γ denotes the angle between the local tangent to the streamline and the downvalley direction x, ϑ the angle between the local tangent to the channel axis and the x direction and α represents the local deviation of streamlines from the channel axis. The angle α can be expressed as a function of the depth-averaged flow field (U, V)

$$\alpha(s, \hat{n}) = \arctan\left(\frac{V}{U}\right), \tag{3.17}$$

which leads to the following dimensionless relationship for streamline curvature $\mathscr{C}_s$:

$$\epsilon \mathscr{C}_s = \nu\mathscr{C} - \frac{UV_{,s} - VU_{,s}}{U^2 + V^2}. \tag{3.18}$$

On substituting (3.15) into (3.1)–(3.4) and depth-averaging, the momentum conservation, flow and sediment continuity in a meandering channel with longitudinally variable width finally read:

$$UU_{,s} + VU_{,n} + H_{,s} + \beta\frac{\tau_s}{D} + f_\alpha = \nu f_{10} + \delta f_{01} + \nu\delta f_{11}, \tag{3.19}$$

$$UV_{,s} + VV_{,n} + H_{,n} + \beta\frac{\tau_n}{D} + g_\alpha = \nu g_{10} + \delta g_{01} + \nu\delta g_{11}, \tag{3.20}$$

$$(DU)_{,s} + (DV)_{,n} = \nu m_{10} + \delta m_{01}, \tag{3.21}$$

$$q_{s,s} + q_{n,n} = \nu p_{10} + \delta p_{01}, \tag{3.22}$$

where (U, V) denotes the depth-averaged velocity vector, H is the free surface elevation and D is local depth. The near-bed shear stress vector (τ_s, τ_n) is modelled as aligned with the near bed velocity vector and can be expressed in terms of a local friction coefficient C_f through the following relationships:

$$(\tau_s, \tau_n) = C_f|\boldsymbol{U}|\,(U, \tau_N + \tau_H), \tag{3.23}$$

$$(\tau_N, \tau_H) = C_f|\boldsymbol{U}|(V, \tau_k), \tag{3.24}$$

$$\tau_k = \epsilon\left[\frac{U\mathscr{C}_s D}{\beta\sqrt{C_{f0}}}\left(k_3 + \frac{k_5 D_{,s}}{\beta\sqrt{C_{f0}}}\right) + \frac{k_4 D^2 (U\mathscr{C}_s)_{,s}}{\beta^2 C_{f0}}\right], \tag{3.25}$$

$$|\boldsymbol{U}| = (U^2 + V^2)^{1/2}. \tag{3.26}$$

Note that the lateral shear stress τ_n is the sum of two contributions, the first due to secondary flows (τ_H) and the second due to the depth-averaged lateral velocity V (τ_N). Moreover, in the expression for τ_H, the quantity $\epsilon\mathscr{C}_s$ appears instead of $\nu\mathscr{C}$ (see

https://doi.org/10.1017/jfm.2011.200 Published online by Cambridge University Press

(4.12) in Zolezzi & Seminara 2001), while k_3, k_4 and k_5 are identical to those reported in Zolezzi & Seminara (2001) (see figure 3) . When stretching the transverse variable with the local value of channel width, s-derivatives in (3.25) must be evaluated according to the chain rule (3.10). Lateral boundary conditions to be associated with (3.19)–(3.22) impose that the lateral walls must be impermeable both to fluid and to sediments, analogously to (3.14):

$$(U, V)\cdot\hat{\boldsymbol{n}}_b = (q_s, q_n)\cdot\hat{\boldsymbol{n}}_b = 0 \quad (n = \pm 1). \tag{3.27}$$

In (3.19)–(3.22), the terms $(f_{ij}, g_{ij}, m_{ij}, p_{ij})$ express the forcing effects of curvature and width variations on the altimetric and flow response at different (ij)th orders of approximations. Considering only terms relevant for the present analysis, the forcing effect of curvature is due to the first $O(\nu)$ terms and it would also appear in meandering channels with constant width. Channel width variations force the system in the form of a first-order contribution $O(\delta)$ that coincides with that corresponding to a straight channel with variable width. Moreover, the $O(\nu\delta)$ term represents the mixed forcing due to width and curvature variations, an effect which therefore is present only in meandering channels with longitudinal width variations. The long algebraic expression of the functions $f_{ij}, \ldots, p_{ij}$ and g_α, f_α are reported in the Appendix that is available as online supplementary material at journals.cambridge.org/flm. The terms g_α and f_α are related to the adopted secondary flow parameterization. They would vanish if channel axis curvature would be used instead of streamline curvature to parameterize centrifugal effects.

The problem formulation is completed by suitable closure relationships to evaluate friction and sediment transport rates. A standard logarithmic law is employed to relate the local friction coefficient to local flow properties

$$C_f = \left[6 + 2.5\,\ln\left(\frac{D}{2.5d_s}\right)\right]^{-2}. \tag{3.28}$$

Sediment transport is assumed to be determined by local flow conditions and also by gravity effects that deviate the sediment particle trajectory from the direction of the mean bottom stress. Bedload rates in the longitudinal and lateral directions (q_s, q_n) are therefore obtained according to the following expressions in the unstretched dimensionless system $(s, \hat{n})$:

$$q_s = \Phi\left\{\cos\delta_q\left[1 - \frac{1}{2}\left(\frac{\eta_{,s}}{\beta(1+\nu\hat{n}\mathscr{C})}\right)^2\right] - \sin\delta_q\left(\frac{\eta_{,s}\,\eta_{,\hat{n}}}{\beta^2(1+\nu\hat{n}\mathscr{C})}\right)\right\}, \tag{3.29}$$

$$q_n = \Phi\sin\delta_q\left[1 - \frac{1}{2}\left(\frac{\eta_{,\hat{n}}}{\beta}\right)^2\right], \quad \sin\delta_q = \left(\frac{\tau_n}{|\boldsymbol{\tau}|} - \frac{r}{\beta\sqrt{\tau_*}}\eta_{,\hat{n}}\right), \tag{3.30}$$

where the angle δ_q quantifies the deviation of the bedload vector from that of the bed shear stress due to the local bed slope in the longitudinal and lateral directions, $\eta = F_0^2 H - D$ represents the local bed elevation and r is an empirical coefficient in the range 0.5–0.6 (Talmon, Struiksma & Van Mierlo 1995). The dimensionless equilibrium bed load function $\Phi(\tau_*)$ is evaluated locally and quantified through the formula of Parker (1990).

https://doi.org/10.1017/jfm.2011.200 Published online by Cambridge University Press

4. Perturbation solution

According to the analysis presented in § 2, the effect of spatial width variations on meander bend stability can be conveniently investigated using a two-parameters (ν and δ) perturbation approach and referring to a regular sequence of sine-generated meander bends, with periodic distributions of channel curvature and width expressed by (2.2) and (2.12), respectively. The unknown variables are therefore expanded as follows:

$$(U, V, H, D) = (1, 0, H_0, 1) + \nu\,[(U_{10}, V_{10}, H_{10}, D_{10})e_1 + \text{c.c.}] + \delta\,[(U_{01}, V_{01}, H_{01}, D_{01})e_2 + \text{c.c.}] + \nu\delta\,[(U_{11}, V_{11}, H_{11}, D_{11})e_1 + \text{c.c.}], \quad (4.1)$$

where only the relevant orders of approximation for the present work ($\nu, \delta, \nu\delta$) have been reported. Assuming $\lambda_w = 2\lambda$, (2.10) implies that one nonlinear interaction at $O(\nu\delta)$ between the linear symmetrical and antisymmetrical solutions is able to reproduce the effect of width variations on the uniform-width bend stability. Note that the nonlinear interaction between the solutions at $O(\nu)$ and at $O(\delta)$ also produces a third longitudinal harmonic in the $O(\nu\delta)$ solution, which can be written as

$$\nu\delta\left[\left(U_{11}^{(3)}, V_{11}^{(3)}, H_{11}^{(3)}, D_{11}^{(3)}\right)e_3 + \text{c.c.}\right]. \quad (4.2)$$

Having a different longitudinal wavenumber than the fundamental harmonic e_1, this third harmonic contribution does not produce a primary effect on bend stability, and will not be analysed in detail in the present paper. Nevertheless, it is worth pointing out that it might play a relevant role in the planform evolution of meander bends, because third longitudinal harmonics typically develop also in uniform-width meandering channels due to geometric (Seminara *et al.* 2001) and flow (Seminara & Tubino 1992) nonlinearities.

Substituting (4.1) into (3.19)–(3.22) and (3.27), a series of ordinary differential systems is obtained, which takes the following form, bold characters denoting vectors:

$$\boldsymbol{L}(\boldsymbol{V}_{1j}) = \boldsymbol{b}_{1j}(n), \quad \boldsymbol{V}_{1j} = (U_{1j}, V_{1j}, H_{1j}, D_{1j}), \quad j = (0, 1), \quad (4.3)$$

$$\boldsymbol{L} = \begin{pmatrix} a_1 & a_2\dfrac{\mathrm{d}}{\mathrm{d}n} & a_3 & a_4 \\ 0 & a_5 & a_6\dfrac{\mathrm{d}}{\mathrm{d}n} & 0 \\ a_7 & a_8\dfrac{\mathrm{d}}{\mathrm{d}n} & 0 & a_9 \\ a_{10} & a_{11}\dfrac{\mathrm{d}}{\mathrm{d}n} & a_{12}\dfrac{\mathrm{d}^2}{\mathrm{d}n^2} & a_{13} + a_{14}\dfrac{\mathrm{d}^2}{\mathrm{d}n^2} \end{pmatrix}, \quad \boldsymbol{b}_{1j} = \begin{pmatrix} b_1^{1j}(n) \\ b_2^{1j}(n) \\ b_3^{1j}(n) \\ b_4^{1j}(n) \end{pmatrix}. \quad (4.4)$$

The coefficients a_k ($k = 1, \ldots, 14$), together with the structure of the forcing terms b_l^{1j} ($l = 1, \ldots, 4$) are reported in Luchi (2009) and can be made available by the Authors upon request. Lateral boundary conditions (3.27) take the form ($j = 0, 1$):

$$\left(V_{1j}, \frac{\mathrm{d}\left(F_0^2 H_{1j} - D_{1j}\right)}{\mathrm{d}n}\right) = \pm\left(b_5^{1j}, b_6^{1j}\right), \quad n = \pm 1, \quad (4.5)$$

while periodic boundary conditions are imposed in the longitudinal domain as suggested by the adopted regular channel geometry. The system (4.3) and (4.5) is reduced to one fourth-order linear ordinary problem for the lateral velocity

https://doi.org/10.1017/jfm.2011.200 Published online by Cambridge University Press

perturbation V_{1j} which can be given an analytical solution in closed form

$$\frac{\mathrm{d}^4 V_{1j}}{\mathrm{d}n^4} + \Gamma_1 \frac{\mathrm{d}^2 V_{1j}}{\mathrm{d}n^2} + \Gamma_2 V_{1j} = \Gamma_0^{1j}(n), \tag{4.6}$$

$$\left(V_{1j}, \frac{\mathrm{d}^2 V_{1j}}{\mathrm{d}n^2} \right) = \pm \left(b_5^{1j}, \Gamma_3^{1j} \right); \quad n = \pm 1, \tag{4.7}$$

where the forcing term $\Gamma_0^{1j}(n)$ as well as the boundary conditions are laterally symmetrical. This forces a laterally symmetrical pattern of V_{1j} which, once substituted into (4.3), determines an antisymmetric structure of the bed profile $\eta_{1j} = F_0^2 H_{1j} - D_{1j}$ and of the longitudinal flow field U_{1j}. The solution procedure is formally identical to that of Blondeaux & Seminara (1985), although with some differences in the governing equations.

The system (4.6) displays the typical features of a forced-damped linear oscillator. Therefore, for given values of (τ_*, d_s), the solution at each order of approximation $(\nu, \delta, \nu\delta)$ shows a resonant behaviour when the spatial frequency of the forcing term coincides with the free longitudinal modes of the system at a given 'resonant' value of the channel width ratio. Exact resonance conditions would imply a theoretically infinite response that is not exhibited by real river systems. Nevertheless, nonlinear analysis (Seminara & Tubino 1992) has demonstrated that close to resonance the system response is typically amplified.

The laterally antisymmetrical perturbation of the near-bank longitudinal velocity $U(s, n = 1)$ associated with the fundamental longitudinal frequency of channel curvature is the part of the solution relevant to bend stability, according to (2.1). It reads:

$$\begin{aligned} U(s, n = 1) &= \nu [U_{10}(n = 1) + \delta U_{11}(n = 1)] \, \mathrm{e}^{(\mathrm{i}\lambda s)} + \mathrm{cc.} \\ &= 2\nu |(U_{10}(n = 1) + \delta U_{11}(n = 1))| \cos(\lambda s + \phi_u), \end{aligned} \tag{4.8}$$

$$\phi_u = \arctan \left(\frac{u_I}{u_R} \right) \tag{4.9}$$

with ϕ_u the phase lag between the location of the peak near-bank excess velocity and the bend apex, and (u_R, u_I) the real and imaginary parts of the complex number $U_{10} + \delta U_{11}$, respectively.

5. Results

Comparing the properties of the solution at $O(\nu\delta)$ and at $O(\nu)$ allows a first theoretical understanding of the effect of width variations on the bend stability mechanism. A first important feature of the longitudinal velocity perturbation is its laterally antisymmetrical structure, as shown in figure 6, where the eigenfunctions $U_{10}(n)$ and $U_{11}(n)$ at $O(\nu)$ and $O(\nu\delta)$ are plotted. The maximum $O(\nu)$ excess velocity across the whole section occurs at the banks, while the cross-sectional maximum of the $O(\nu\delta)$ correction due to width variations can be slightly shifted towards the channel centreline, although it still remains close to the bank regions. This implies that the lateral wavelength of $U_{11}(n)$ can be slightly smaller with respect to that of $U_{10}(n)$.

The relationship between bend stability and the position of the peak near-bank excess velocity along one meander wavelength is illustrated in figure 7. Bank erosion tends to amplify the bend when the migration rate ζ (and therefore $U(s, n = 1)$, according to (2.1)) peaks in the unstable region of figure 7. Bends are therefore

https://doi.org/10.1017/jfm.2011.200 Published online by Cambridge University Press

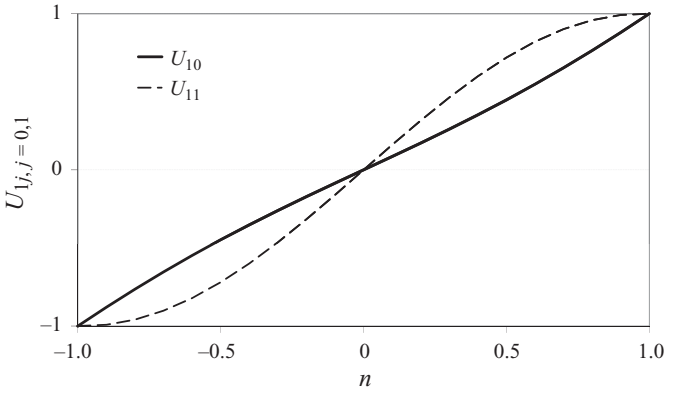


FIGURE 6. Transverse profile of the perturbations of the longitudinal velocity U_{10} and U_{11} in $s = 0$ ($\beta = 10; \tau_* = 0.1; d_s = 0.01; \lambda = 0.1; \omega = 0$). The values are scaled with the maximum value at each order.

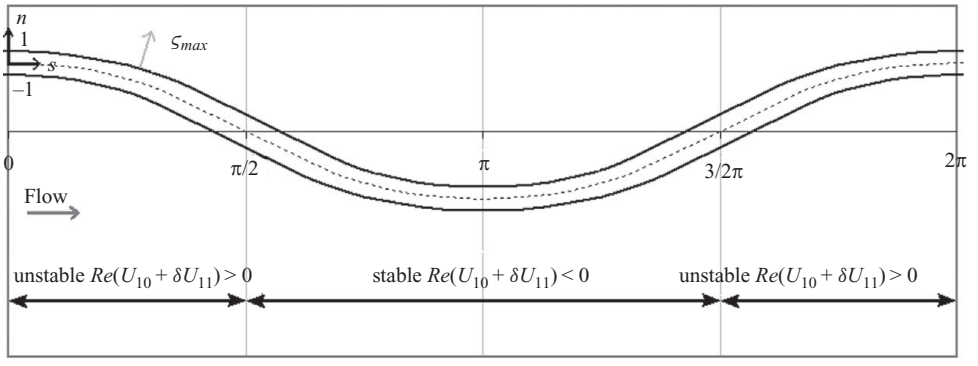


FIGURE 7. Conceptual diagram of bend stability, which is controlled by the position of the maximum lateral migration rate ζ_{max}. For positive near-bank values of $Re(U_{10} + \delta U_{11}(n = 1))$, the meander is planimetrically unstable and eventually tends to grow, while when $Re(U_{10} + \delta U_{11}(n = 1)) < 0$ the maximum migration rate is positioned along a convex inner bend ($\pi/2 < \phi_u < 3\pi/2$) and the meander tends to be straightened.

unstable for values of the phase lag ϕ_u (see (4.8)) in the ranges $(0, \pi/2)$ and $(3\pi/2, 2\pi)$. The phase lag ϕ_u is related to the sign of the real part u_R of the complete solution $(U_{10} + \delta U_{11})$, with positive values of u_R implying bend amplification (figure 7). It is therefore necessary to compare the behaviour of the real part of the near-bank longitudinal velocity at both $O(\nu)$ and $O(\nu\delta)$.

Figure 8 shows the dependence of the real parts of $U_{10}(n = 1)$ and of $U_{11}(n = 1)$ on the meander wavenumber λ for two different values of the aspect ratio β and when width variations are in phase with channel curvature ($\omega = 0$, (2.12)).

Three different scenarios can be observed for a given combination of the governing parameters (β, τ_*, d_s). For relatively long meander bends (small values of λ), the two solutions have the same positive sign, which means that width variations reinforce an instability process that occurs also with uniform width. Almost invariably, a different scenario occurs when λ increases: the solutions at the two orders of approximation have contrasting sign, most frequently with the $O(\nu\delta)$ solution being positive. Therefore, depending on the intensity δ of width variations, the wavenumber range that is unstable when the width is uniform widens towards higher values of λ.

https://doi.org/10.1017/jfm.2011.200 Published online by Cambridge University Press

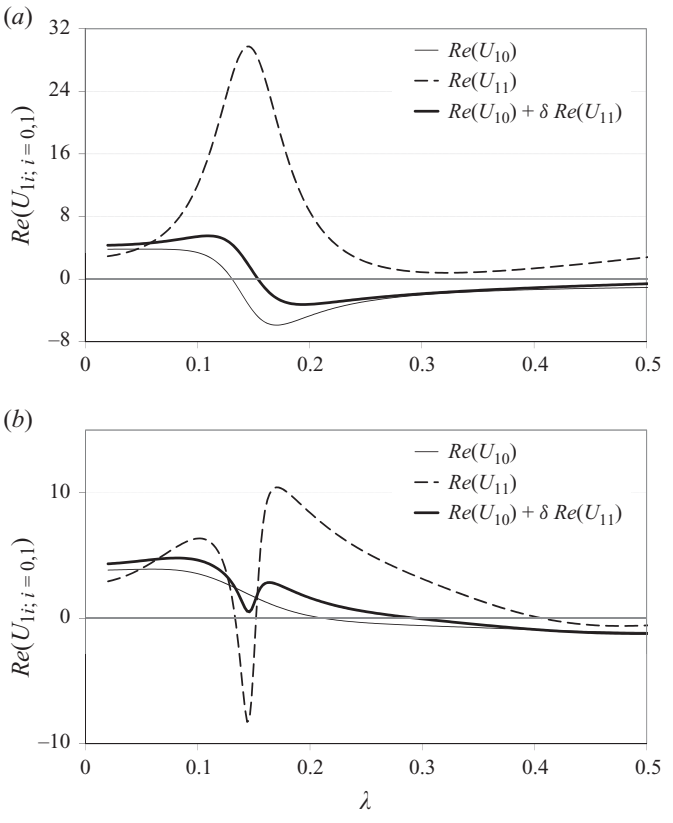


FIGURE 8. Dependence of the real part of the near-bank longitudinal excess velocity U on the meander wavenumber λ at different orders of approximation and for the complete solution. ($\tau_* = 0.08$; $d_s = 0.04$; $\omega = 0$; $\delta = 0.17$ and (*a*) $\beta = 8$; (*b*) $\beta = 20$).

This means that spatial width variations tend to promote the instability of shorter meanders that are stable when channel width is constant. Looking at figure 8(*b*), a third configuration appears, whereby width variations tend to stabilize meanders that are expected to grow with constant channel width. This latter scenario is associated with the minimum in the dashed curve that corresponds to the $O(\nu\delta)$ solution but it is normally restricted to relatively small λ and β ranges.

Comparing figure 8(*a*) with figure 8(*b*), another interesting behaviour appears. For $\beta = 20$ (figure 8*b*), the minimum in the $O(\nu\delta)$ solution separates two distinct unstable wavelength ranges with different peaks in the $Re(U_{11})(\lambda)$ curve, a feature which is neither present at lower values of β (figure 8*a*) nor when the width is constant (thin continuous line). Depending on the value of δ, this may give rise to two rather distinct unstable longitudinal modes in the complete solution, thus suggesting a rather different dynamics with respect to meanders with constant width, where invariably one well-defined unstable range develops. The presence of two distinct peaks at relatively higher values of β in the $O(\nu\delta)$ solution can be related to the resonance properties at the different orders of approximation, determined by the homogeneous part of the governing linear differential problem (4.6). Blondeaux & Seminara (1985) showed that if (λ_R, β_R) denotes the resonant conditions for the meandering channel with uniform width $O(\nu)$, resonance will also occur for $(\lambda, \beta) = m(\lambda_R, \beta_R)$, with m

https://doi.org/10.1017/jfm.2011.200 Published online by Cambridge University Press

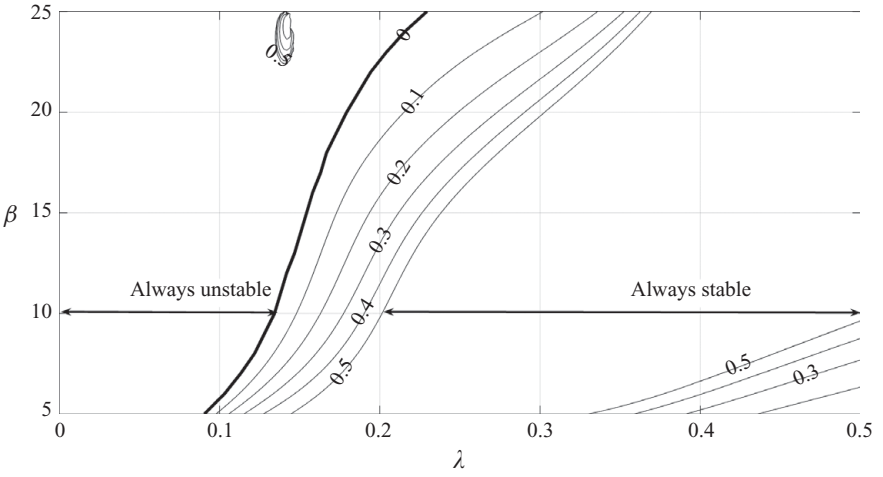


FIGURE 9. Marginal bend stability curves for different values of δ. ($\tau_* = 0.09; d_s = 0.03; \omega = 0$).

being an integer. Since the adopted wavelength ratio $\lambda = 2\lambda_w$ (see (2.10)), the $O(\delta)$ solution hence resonates at $(\lambda_R, 2\beta_R)$. The $O(\nu\delta)$ solution has the same longitudinal structure of the $O(\nu)$ solution and therefore resonates at (λ_R, β_R), which is associated with one of the two peaks. The second peak, appearing at relatively high values of β, is related to the reminiscence of resonant conditions of the $O(\delta)$ $(\lambda_R, 2\beta_R)$ embedded in the forcing term, because this results from the nonlinear interaction between the two linear solutions.

Equation (4.8) indicates that the ultimate ability of width variations to reverse the stability properties of constant-width meander bends is a combination of the shape of the two solutions and of the magnitude of width variations δ, because $u_R = U_{10} + \delta U_{11}$. A more complete picture can be obtained by plotting neutral stability curves for the complete solution u_R in the $(\lambda$–$\beta)$ plane, which separates stable and unstable regions for given values of the Shields stress τ_* and of the relative roughness d_s.

Figure 9 shows an example of neutral bend stability curves corresponding to different amplitudes δ of width variations in phase with channel curvature ($\omega = 0$). The thick line refers to the limit case of meanders with constant width ($\delta = 0$): long meander bends are unstable and the instability range extends towards shorter wavelengths for increasing values of the width ratio (Zolezzi *et al.* 2009*b*). The other curves correspond to increasing amplitude of width variations: for instance, $\delta = 0.17$ means that channel width in the widest section is nearly twice that of the narrowest section, while $\delta = 0.5$ represents the upper geometrical limit whereby the width of the narrowest section vanishes. The shift of the neutral curves towards larger values of λ as δ increases reveals that for values of the width ratio β typical of natural single-thread streams (between 5 and 25 in figure 9), width variations invariably promote the instability of shorter bends, which would otherwise be stable if the channel width was uniform. On the contrary, longer bends that are unstable with uniform width do not change their stability condition except for a relatively small β range (between 23 and 25 in figure 9) when the observed minimum peak of the $O(\nu\delta)$ correction is large enough to stabilize a restricted wavelength range. As already noted, such behaviour generally results in localized effects that do not significantly contribute to the overall picture.

https://doi.org/10.1017/jfm.2011.200 Published online by Cambridge University Press

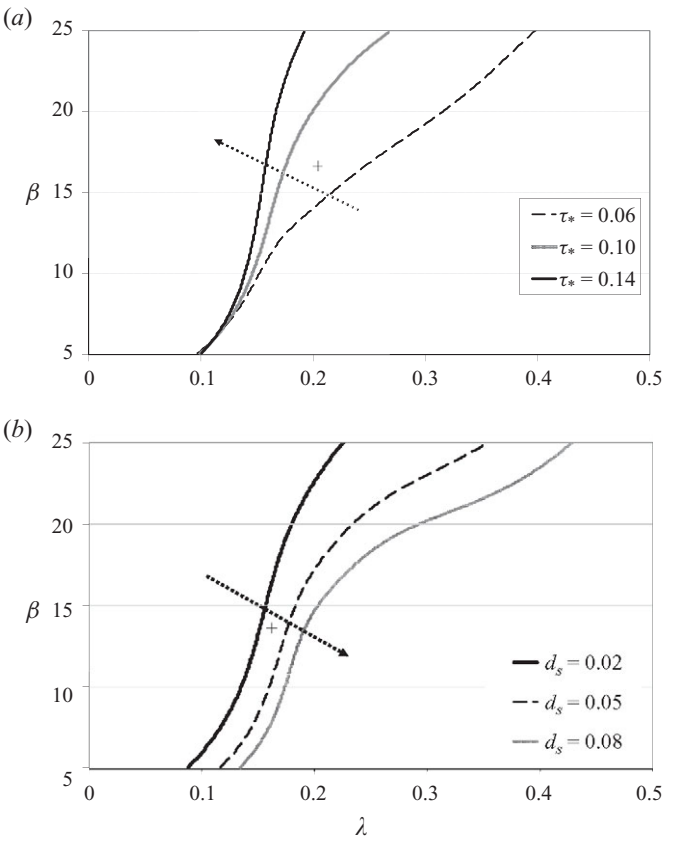


FIGURE 10. Marginal stability curves in the (λ–β) plane for different values of (*a*) τ_* ($d_s = 0.03$, $\omega = 0$, $\delta = 0.1$) and (*b*) d_s ($\tau_* = 0.1$, $\omega = 0$, $\delta = 0.1$).

It is interesting to examine how the stability process is controlled by the reach-averaged Shields stress τ_* and relative roughness d_s. Figures 10(*a*) and 10(*b*) show neutral curves of bend stability corresponding to different values of τ_* and d_s, respectively, for width oscillations in phase with curvature and amplitude $\delta = 0.1$. Higher reach-averaged formative Shields stresses (figure 10*a*) promote the instability of longer bends and tend to stabilize the shorter ones. When examining the variation of the relative roughness d_s, a somewhat consistent behaviour emerges, although the two parameters are treated as mutually independent. Namely, also meanders with smaller relative roughness tend to promote the instability of longer bends, with a more pronounced trend for larger width oscillations. Both behaviours parallel that of the $O(\nu)$ solution obtained with a homogeneous width.

Figure 3(*b*) indicates that the widest section in a meander bend can both anticipate or follow the bend apex, for a distance that is usually less than half the bend length. The presence of a phase lag ω between the widest and most curved cross-section modifies the picture previously described. Indeed, a new factor ($e^{i\omega}$, see (2.12)) appears in the forcing terms and it produces a sinusoidal effect (with period π) in the $O(\nu\delta)$ response: for instance, opposite behaviours (stable versus unstable) apply for $\omega = \pi/4$ and for $\omega = -\pi/4$. In this way, the relative lag ω between the two planform forcings affects the shape and the amplitude of the solution and therefore the whole bend stability mechanism. This effect can be examined by referring to

https://doi.org/10.1017/jfm.2011.200 Published online by Cambridge University Press

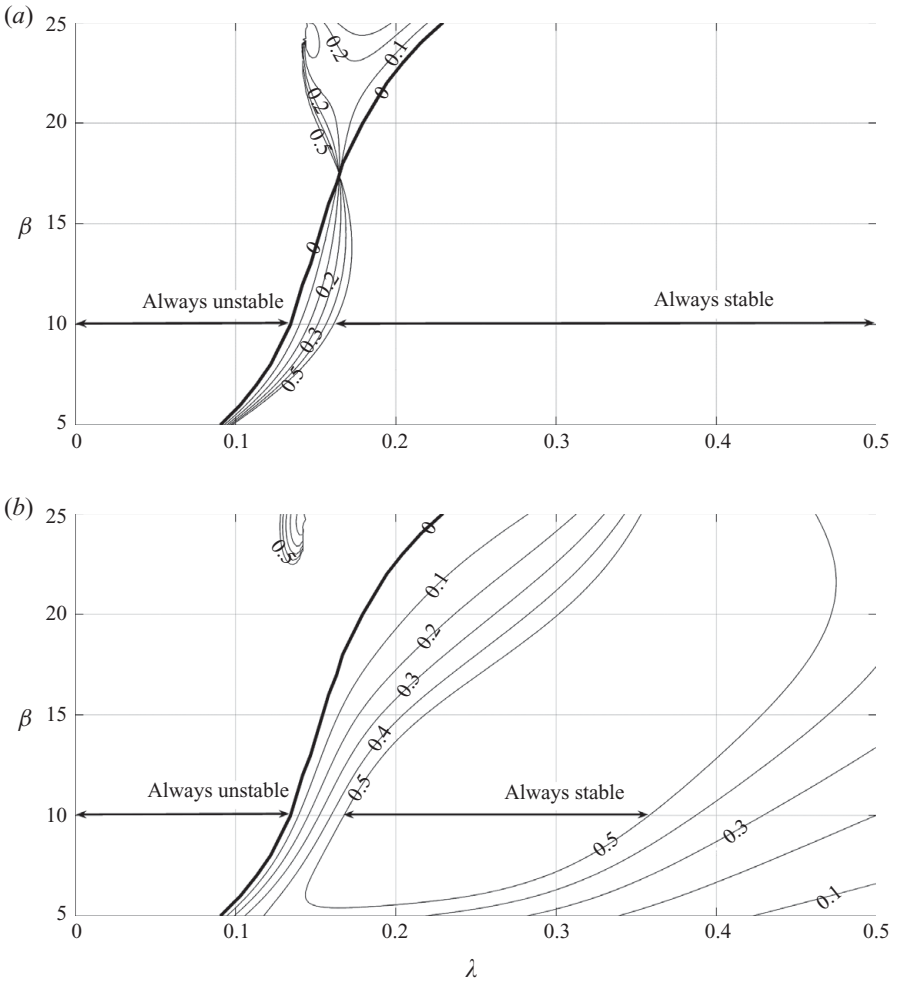


FIGURE 11. Dependence of the neutral stability curves from the phase lag ω between curvature and width variations. $\tau_* = 0.09$; $d_s = 0.03$ and (*a*) $\omega = \pi/4$; (*b*) $\omega = -\pi/8$.

the neutral stability curves plotted in figures 11(*a*) and 11(*b*), together with those in figure 9. Neutral curves in figures 11(*a*) and 11(*b*) correspond to the widest section, respectively, located upstream ($\omega = \pi/4 > 0$) and downstream ($\omega = -\pi/8 < 0$) the bend apex. The same combination of the governing parameters of figure 9 ($\omega = 0$) has been used to compare the solution at three different values of ω. When the widest section in a meander bend is progressively shifted downstream, width variations increasingly destabilize shorter bends. When the width maximum is upstream of the bend apex, width variations of increasing amplitude stabilize relatively long bends that are unstable at $O(\nu)$ for values of β between 17 and 25. This behaviour tends to be reversed when the width peak progressively moves downstream (figure 9, $\omega = 0$ and figure 11(*b*), $\omega = -\pi/8 < 0$), i.e. when the instability region includes also shorter meanders with respect to the uniform-width bend theory. Furthermore, when the widest section is located downstream of the bend apex, relatively short bends may become unstable for large-enough width variations, with comparable wavelengths to

https://doi.org/10.1017/jfm.2011.200 Published online by Cambridge University Press

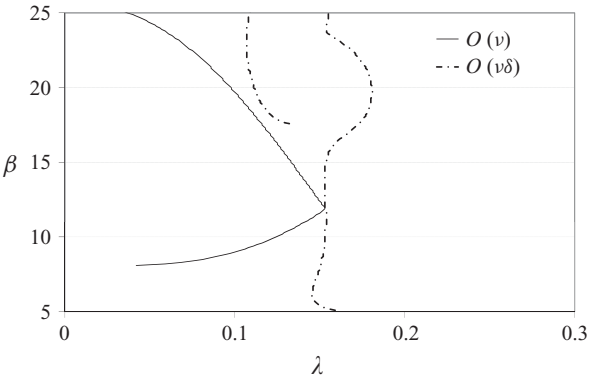


FIGURE 12. Wavenumber with maximum of the real part of the longitudinal velocity at the banks U as function of β at different orders of approximation ($\tau_* = 0.1$, $d_s = 0.05$, $\omega = 0$).

those of the bar instability process ($\lambda \sim 0.4$) (Blondeaux & Seminara 1985; Colombini *et al.* 1987).

Also, the tendency of the $O(\nu\delta)$ solution to develop two most unstable longitudinal modes can be examined in more detail in the (λ–β) plane to better understand the potential implications for meander wavelength selection. The most unstable meander wavenumbers λ_{max} at $O(\nu)$ and $O(\nu\delta)$ are reported in figure 12 as functions of the channel aspect ratio β, for width variations in phase with the curvature distribution. Coherently with the extension of the unstable range towards larger values of λ, the most unstable meander wavelengths associated with the nonlinear correction are shorter ($0.15 < \lambda_{max} < 0.2$) with respect to the uniform case, for which $\lambda_{max} < 0.15$ (solid curve in figure 12). For large-enough aspect ratios β, moreover, a second peak in the $O(\nu\delta)$ response appears with a closer wavelength to the uniform $O(\nu)$ solution. The actual presence of two unstable longitudinal modes in the complete solution $U = U_{10} + \delta U_{11}$ will ultimately depend on the shape of the solutions at the two orders of approximation, and on the value of δ.

6. Discussion

Relatively few field and experimental investigations are presently available to be directly compared with the outcomes of the present bend theory. This notwithstanding, it is useful to frame the key features of the present analysis in the context of existing field, experimental and theoretical work. The present discussion has therefore three main objectives: (i) to place the present approach into a broader theoretical perspective involving the study of river morphodynamics with spatial variations of both channel width and curvature; (ii) to assess the suitability of the proposed bend theory to replicate observed features, at least considering average behaviours and (iii) to discuss the physical implications of the presence of multiple most unstable longitudinal modes associated with the interactions between spatial curvature and width variations.

A basic element of the present bend theory is that one nonlinear interaction between the linear responses at $O(\nu)$ and $O(\delta)$ is enough to reproduce the main effect of width variations on bend stability. By analysing the mixed $O(\nu\delta)$ response, the present analysis introduces a rather novel perspective (see Solari & Seminara 2005 for an

https://doi.org/10.1017/jfm.2011.200 Published online by Cambridge University Press

earlier attempt) in modelling river morphodynamics, according to which meanders are systems governed by the presence of two mutually interacting planform forcing effects, namely the spatial variations of channel curvature and width. The present work focuses on the one-way effect of width variations on bend stability, i.e on channel curvature. We have assumed known amplitude, wavelength and phase lag of width variations and we have not focused on the possible causes for their development within meandering rivers. A theoretical investigation of the reciprocal effect of curvature on the development of spatial width variations has recently been proposed by Luchi *et al.* (2010*b*). On the basis of a perturbation solution of the same governing differential system of the present analysis, two physical mechanisms are indicated by Luchi *et al.* (2010*b*) as possibly being responsible for the presence of spatial width variations in meanders: a laterally symmetrical and a laterally antisymmetrical mechanism. The former mechanism is due to the prior presence of mid-channel bars that can develop due to nonlinear self-interactions, at $O(\nu^2)$, in uniform-width meanders and that can symmetrically force the flow towards both banks thus inducing local widening. The latter mechanism is associated with the different lateral migration rates of opposite banks at a cross-section, when they are subject to the different physical processes of bank accretion and erosion. This latter mechanism still needs further exploration, particularly because very little is still known about the physics of bank accretion. Parker *et al.* (2011) have recently proposed a novel approach to model the effect of the dynamic interaction between opposite bank processes on channel width. Existing work nevertheless suggests that flow nonlinearities shall be taken into account in mathematical models aiming at predicting the coupled effect of curvature and width variations on meander morphodynamics (Zolezzi, Luchi & Tubino 2009*a*). Flow nonlinearity has already been shown to also affect meander wavelength selection when channel width is uniform, by introducing a dependence of the selected meander wavelength from the initial meander amplitude (Bolla Pittaluga *et al.* 2009).

The second objective of the present discussion is to make a preliminary test of the ability of the present bend theory to replicate observed behaviours. The present analysis predicts a consistent tendency of channel width variations to promote the instability of relatively short bends that are stable when the channel width is uniform. With respect to meanders with uniform width, this behaviour emerges (i) from the extension of the unstable meander range towards shorter wavenumbers (figures 9 and 11) and (ii) from the development of shorter most unstable modes at the first nonlinear interaction ($O(\nu\delta)$, figure 12). The opposite scenario can be found only for narrow ranges of the spatial lag ω between the widest and the most curved section (figure 11*a*), which can therefore be viewed as an exception to the general behaviour. The predicted tendency is consistent with the significant wavelength difference emerging from figure 1. The mean wavenumber values are 0.21 for class B_1 and 0.26 for class C; application of a t-test indicates that their difference is significant with more than 99% probability.

The comparison between the two classes reported in figure 1 has been performed as follows. Figure 1 compares 1281 'wider-at-bends' (C) and 707 'equiwidth' (B_1) meander bends according to Lagasse *et al.* (2004) classification. Each class contains bends belonging to the same river, and data for almost each bend refers to three different dates with nearly 20-years intervals among one another. Bends belonging to a total of 63 class C ad 20 class B_1 river reaches are compared. This difference still appears and is significant also when restricting the comparison to a single date for each bend. This comparison therefore supports the predicted tendency of meanders

https://doi.org/10.1017/jfm.2011.200 Published online by Cambridge University Press

with width variations to develop shorter bends compared to those with spatially uniform channel width.

The last aim of the present section is to discuss the physical implications of the predicted presence of two unstable longitudinal modes (figures 8 and 12), which correspond to two distinct, almost equally unstable values of meander wavenumber λ. The present theory predicts that this occurs for some combinations of the governing parameters and invariably at values of β larger than $10 \div 15$ for typical bankfull conditions of gravel-bed rivers. The same two peaks are evident in the curve corresponding to the real part of U_{11} in figure 8(b), where the most unstable wavenumbers at the $O(\nu\delta)$ are $\lambda_1 \sim 0.102$ and $\lambda_2 \sim 0.17$. Figure 8(b) also suggests that this can also be reflected in the complete solution (4.8) with these two meander wavelengths eventually achieving equal bend instability for δ only slightly larger with respect to the value used in figure 8(b) ($\delta = 0.17$), corresponding to the widest section being twice as large as the narrowest section.

This behaviour represents a marked difference with uniform-width meanders, for which bend instability is characterized by the presence of a single unstable longitudinal mode. Meanders with intense-enough spatial width variations, and at sufficiently large bankfull aspect ratios, might therefore display a long-term tendency towards almost two different equally unstable planforms characterized by well distinct meander wavelengths. The longer wavelength is close to the most unstable one with uniform width, while the shorter most unstable wavelength is associated with nonlinear interactions between curvature and width variations.

This observation can be put in qualitative relationship with the observed reach-scale tendency of some meandering rivers to develop chute cutoffs. The meander bend classification of Lagasse *et al.* (2004), based on Brice (1975), recognizes that some meandering rivers with intense spatial width variations are frequently characterized by a consistent tendency to develop chute cutoffs at a reach scale (type *D* in Lagasse *et al.* 2004's classification). A meandering planform with frequent presence of chute channels can be visually interpreted as resulting from two superposed meandering channels with different intrinsic wavelengths ($\lambda_1 < \lambda_2$) and similar Cartesian wavelengths. On the basis of the present theoretical outcomes, these meandering planforms may reflect an intrinsic long-term dynamics whereby meander wavelength selection is controlled by a delicate competition between two nearly equally unstable longitudinal modes λ_1 and λ_2.

7. Concluding remarks

Most mathematical models of river meander dynamics assume channel width to be constant in space. A systematic quantification of spatial width variations in meanders and of their dynamic effects is lacking so far, both from field observations and from theoretical approaches. The present paper revisits the classical, uniform-width bend theory (Hasegawa 1977; Ikeda *et al.* 1981) in order to make a first step in understanding whether and how spatial width oscillations can be expected to control the process of linear bend stability that initiates meander planform evolution. The theory is developed by assuming that the morphodynamics of meandering rivers is related to two forcing effects, namely those of spatial curvature and width variations. A preliminary quantification of the key features of width variations (spatial frequency, amplitude, location along a meander bend) in a freely evolving meandering river allows the substantiation of two main assumptions of the present modified bend theory. First, the dimensionless amplitude δ of width variations is a 'small' parameter

https://doi.org/10.1017/jfm.2011.200 Published online by Cambridge University Press

with comparable magnitude to that (ν) of curvature variations ($\sim O(0.1)$). Second, it is consistent with field observations to assume that the frequency of width variations is twice that of curvature. This allows the formulation of a two-parameters perturbation expansion in terms of the small parameters ν and δ. The peculiar frequency ratio of the two planform forcing effects ($\lambda_w = 2\lambda$) implies that one nonlinear interaction is able to reproduce the longitudinal structure of the fundamental perturbation governing the uniform-width bend stability, thus producing an $O(\nu\delta)$ correction that, thanks to its lateral antisymmetry, quantifies the dynamic effect of spatial width variations on linear bend stability.

The behaviour of the first-order nonlinear interaction between curvature and width variations has been computed for different values of the reach-averaged bankfull hydraulic conditions (β, τ_*, d_s) as a function of the dimensionless meander wavenumber λ for different amplitudes δ of width oscillations and phase lags ω between the widest and the most curved cross-sections. The overall effect of width variations is a consistent tendency to promote the instability of relatively short bends, with dimensionless wavenumbers up to 0.3 for β larger than $15 \div 20$ for typical bankfull conditions of gravel-bed rivers that are stable when the channel width is uniform. This effect is enhanced when the location of the widest section is progressively shifted from upstream to downstream of the bend apex, when the enlargement of the instability range towards higher values of λ is more pronounced. Coherently, the nonlinear correction due to width variations is associated with the shorter most unstable meander wavelength. On average, these theoretical findings are supported by existing field data from a relatively large number of natural meander bends. Under bankfull conditions representative of gravel-bed rivers, when β is larger than $15 \div 20$, the mixed response tends to produce two markedly separated most unstable longitudinal modes λ associated with two distinct peaks in the mixed response $Re(U_{11})$, a behaviour that is absent when the width is uniform. This has been put in qualitative relationship with the reach-scale occurrence of chute cutoffs that has been preferentially observed in meanders with spatial variations of channel width (Lagasse *et al.* 2004 based on Brice 1975).

The present analysis appears of particular relevance for understanding and predicting the planform evolution of a meandering channel with spatially variable width. A deeper understanding of these systems would be of major importance in river morphodynamics because it can help in improving our knowledge of both meandering river dynamics and also of transitional morphologies between meandering and braiding. Although a complete predictive model is still far from being developed, several features of the present work may be particularly relevant for a further understanding of the planform evolution of these systems. The present outcomes indeed indicate the key role of an updated mechanistic view of meandering rivers as natural systems forced by two planform effects that mutually interact: spatial curvature and width variations. Moreover, beyond the analysed outcomes of the theory, the observed tendency of spatial width variations to stimulate the evolution of third harmonics with respect to the fundamental shall be taken into account. This might imply a more rapid tendency towards skewing and fattening of meander forms when width variations are present, with potentially relevant interaction with the growth of the typical third harmonic that appears in the Kinoshita (1961) curve also due to flow and geometric nonlinearties in constant-width channels. Last but not the least, a major advance in this direction basically requires the availability of more systematic quantifications of the properties of width variations in river meanders possibly highlighting also their dynamic effects.

https://doi.org/10.1017/jfm.2011.200 Published online by Cambridge University Press

The work has been supported by the RIMOF2 project, financed by the Fondazione CaRi Verona, Vicenza, Belluno e Ancona and by the projects 'Morphodynamical processes in river and riparian ecosystems—PRIN 2006' and 'Hydrodynamic transport processes and biomorphodynamics of river corridors'—PRIN 2008, co-funded by the Italian Government (MIUR) and the University of Trento. The authors are thankful to A. Frascati for sharing morphological image processing tools and procedures.

Supplementary material is available at journals.cambridge.org/flm

REFERENCES

Bertoldi, W. & Tubino, M. 2005 Bed and bank evolution of bifurcating channels. *Water Resour. Res.* **41** (7), W07001, doi:10.1029/2004WR003333.

Blanckaert, K. & de Vriend, H. J. 2004 Secondary flow in sharp open channel bends. *J. Fluid Mech.* **498**, 353–380.

Blondeaux, P. & Seminara, G. 1985 A unified bar-bend theory of river meanders. *J. Fluid Mech.* **157**, 449–470, doi:10.1017/S0022112085002440.

Bolla Pittaluga, M., Nobile, G. & Seminara, G. 2009 A nonlinear model for river meandering. *Water Resour. Res.* **45**, w04432, doi:10.1029/2008WR007298.

Brice, J. C. 1975 Air Photo Interpretation of the Form and Behavior of Alluvial Rivers. Final Rep. US. Army Research Office, Washington University, 10p.

Brice, J. C. 1982 Stream channel stability assessment. Rep. No. FHWA/RD. Federal Highway Administration, US Department of Transportation, 42p.

Camporeale, C., Perona, P., Porporato, A. & Ridolfi, L. 2007 Hierarchy of models for meandering rivers and related morphodynamic processes. *Rev. Geophys.* **45** (1), RG1001, doi:10.1029/2005RG000185.

Carling, P. 1988 The concept of dominant discharge applied to 2 gravel-bed streams in relation to channel stability thresholds. *Earth Surf. Process. Landf.* **13** (4), 355–367.

Colombini, M., Seminara, G. & Tubino, M. 1987 Finite-amplitude alternate bars. *J. Fluid Mech.* **181**, 213–232.

Constantine, J. A., McLean, S. R. & Dunne, T. 2010 A mechanism of chute cutoff along large meandering rivers with uniform floodplain topography. *GSA Bull.* **122** (5/6), 855–869, doi:10.1130/B26560.1.

Darby, S. E., Alabyan, A. M. & Van de Wiel, M. J. 2002 Numerical simulation of bank erosion and channel migration in meandering rivers. *Water Resour. Res.* **38** (9), 1163, doi:10.1029/2001WR000602.

Edwards, B. F. & Smith, D. H. 2002 Critical wavelength for river meandering. *Phys. Rev.* E **63**, 045304(R), doi:10.1103/PhysRevE.63.045304.

Ferguson, R. I., Ashmore, P. E., Ashworth, P. J., Paola, C. & Prestegaard, K. L. 1992 Measurements in a braided river chute and lobe. 1. Flow pattern, sediment transport and channel change. *Water Resour. Res.* **28** (7), 1877–1886.

Frascati, A. & Lanzoni, S. 2009 Morphodynamic regime and long-term evolution of meandering rivers. *J. Geophys. Res.* **114**, F02002, doi:10.1029/2008JF001101.

Frascati, A. & Lanzoni, S. 2010 Long-term meandering evolution as part of chaotic dynamics? a contribution from mathematical modelling. *Earth Surf. Process. Landf.* (Special Issue on River Meander Dynamics, ed. J. M. Hooke, E. Gautier and G. Zolezzi) **35** (7), 791–802, doi:10.1002/esp.1974.

Gautier, E., Brunstein, D., Vauchel, P., Roulet, M., Fuertes, O., Darrozes, J. & Bourrel, L. 2007 Temporal relations between meander deformation, water discharge and sediment fluxes, floodplain of the Rio Beni (Bolivian Amazonia). *Earth Surf. Process. Landf.* **32** (2), 230–248.

Hasegawa, K. 1977 Computer simulation of the gradual migration of meandering channels (in Japanese). In *Proceedings of the Hokkaido Branch, Japan Society of Civil Engineering*, pp. 197–202.

Hasegawa, K. 1989 Studies on qualitative and quantitative prediction of meander channel shift. In *River Meandering AGU, Water Resour.* Monogr. (ed. S. Ikeda & G. Parker), vol. 12, pp. 215–235. American Geophysical Union, Washington, DC.

https://doi.org/10.1017/jfm.2011.200 Published online by Cambridge University Press

Hey, R. D. 1982 *Design Equations for Mobile Gravel-Bed Rivers*, (ed. R. D. Hey, J. C. Bathurst & C. R. Thorne), pp. 553–574. Wiley, Chichester, UK.

Hooke, J. M. 1986 The significance of mid-channel bars in an active meandering river. *Sedimentology* **33** (6), 839–850.

Howard, A. D. 1992 Modelling channel migration and floodplain sedimentation in meandering streams. In *Lowland FloodPlain Rivers: Geomorphological Perspectives*(ed. P. A. Carling & G. E. Petts), pp. 1–41. John Wiley & Sons.

Ikeda, S., Parker, G. & Sawai, K. 1981 Bend theory of river meanders. Part 1. Linear development. *J. Fluid Mech.* **112**, 363–377.

Johannesson, H. & Parker, G. 1989 Secondary flow in mildly sinuous channels. *ASCE J. Hydraul. Engng* **115**, 289–308.

Kalkwijk, J. P. Th. & De Vriend, H. J. 1980 Computation of the flow in shallow river bends. *J. Hydraul. Res.* **18** (4), 327–342.

Kinoshita, R. 1961 Investigation of channel deformation in Ishikari River (in Japanese). *Tech. Rep*. Bureau of Resources, Dept. Science and Technology, Japan.

Knighton, A. D. 1972 Changes in a braided reach. *Geol. Soc. Am. Bull.* **83** (12), 3813–3822.

Lagasse, P. F., Spitz, W. J., Zevenbergen, L. W. & Zachmann, D. W. 2004 Handbook for predicting stream meander migration. In *NHCRP Rep. 533*. National Cooperative Highway Research Program, 107 pp.

Langbein, W. B. & Leopold, L. B. 1964 Quasi equilibrium states in channel morphology. *Am. J. Sci.* **262**, 782–794.

Lanzoni, S. & Seminara, G. 2006 On the nature of meander instability. *J. Geophys. Res.* **111**, (F04006), doi:10.1029/2005JF000416.

Luchi, R. 2009 The effect of width and curvature variations on river meander morphodynamics. PhD thesis, Doctoral School in Environmental Engineering, University of Trento.

Luchi, R., Bertoldi, W., Zolezzi, G. & Tubino, M. 2007 Monitoring and predicting channel change in a free-evolving, small Alpine river: Ridanna Creek (North East Italy). *Earth Surf. Process. Landf.* **32** (14), 2104–2119.

Luchi, R., Hooke, J., Zolezzi, G. & Bertoldi, W. 2010*a* Width variations and mid-channel bar inception in meanders: River Bollin (UK). *Geomorphology* **119**, 1–8, doi:10.1016/j.geomorph.2010.01.010.

Luchi, R., Zolezzi, G. & Tubino, M. 2010*b* Modelling mid-channel bars in meandering channels. *Earth Surf. Process. Landf.* (Special Issue on River Meander Dynamics, ed. J. M. Hooke, E. Gautier & G. Zolezzi) **35**, 902–917, doi:10.1002/esp.1947.

Parker, G. 1984 Theory of meander bend deformation. In *River Meandering, Proceedings of the Conference Rivers 1983* (ed. C. M. Elliott), pp. 722–732. American Society of Civil Engineers.

Parker, G. 1990 Surface-based bedload transport relation for gravel rivers. *J. Hydraul. Res.* **28**, 417–436.

Parker, G., Diplas, P. & Akiyama, J. 1983 Meanders bends of high amplitude. *ASCE J. Hydraul. Engng* **109**, 1323–1337.

Parker, G., Sawai, K. & Ikeda, S. 1982 Bend theory of river meanders, Part 2: Nonlinear deformation of finite-amplitude bends. *J. Fluid Mech.* **115**, 303–314.

Parker, G., Shimizu, Y., Wilkerson, G. V., Eke, E. C., Abad, J. D., Lauer, J. W., Paola, C., Dietrich, W. E. & V. R., Voller 2011 A new framework for modeling the migration of meandering rivers. *Earth Surf. Process. Landf.* **36** (1), 70–86. doi:10.1002/esp.2113.

Pizzuto, J. E. & Meckelnburg, T. S. 1989 Evaluation of a linear bank erosion equation. *Water Resour. Res.* **25** (5), 1005–1013.

Repetto, R., Tubino, M. & Paola, C. 2002 Planimetric instability of channels with variable width. *J. Fluid Mech.* **457**, 79–109.

Rinaldi, M. & Darby, S. E. 2007 Modelling river-bank-erosion processes and mass failure mechanisms: progress towards fully coupled simulations. In *Gravel-bed Rivers 6-From Process Understanding to River Restoration. Series Developments in Earth Surface Processes*, (ed. H. Habersack, H. Piegay & M. Rinaldi), vol. 11, pp. 213–239. Elsevier.

Rozovskij, I. L. 1957 Flow of water in bends of open channel. *Tech. Rep*. Acad. Sci. Ukrainian SSR.

https://doi.org/10.1017/jfm.2011.200 Published online by Cambridge University Press

Rüther, N. & Olsen, N. R. B. 2007 Modelling free-forming meander evolution in a laboratory channel using three-dimensional computational fluid dynamics. *Geomorphology*, doi:10.1016/j.geomorph.2006.12.009.

Seminara, G. 2006 Meanders. *Paper invited for the 50th Anniversary issue of the J. Fluid Mech.* **554**, 271–297.

Seminara, G. & Solari, L. 1998 Finite amplitude bed deformations in totally and partially transporting wide channel bends. *Water Resour. Res.* **34** (6), 1585–1594.

Seminara, G. & Tubino, M. 1989 Alternate bars and meandering: Free, forced and mixed interactions. In *River Meandering* (ed. S. Ikeda & G. Parker), pp. 267–320. AGU Water Resour. Monogr 12. American Geophysical Union.

Seminara, G. & Tubino, M. 1992 Weakly nonlinear theory of regular meanders. *J. Fluid Mech.* **244**, 257–288.

Seminara, G., Zolezzi, G., Tubino, M. & Zardi, D. 2001 Downstream and upstream influence in river meandering. Part 2. Planimetric development. *J. Fluid Mech.* **438**, 213–230.

Solari, L. & Seminara, G. 2005 On width variations in meandering rivers. In *Proc. 4th IAHR Symp. River, Coastal and Estuarine Morphodynamics (RCEM 2005)*, 4–7 October, Urbana, IL (ed. G. Parker & M. H. Garcia), vol. 2, pp. 745–751. Balkema.

Stolum, H. H. 1996 River meandering as a self-organisation process. *Science* **271** (5256), 1710–1713.

Sun, T., Meaking, P., Jossang, T. & Schwarz, K. 1996 A simulation model for meandering rivers. *Water Resour. Res.* **32** (9), 2937–2954.

Talmon, A. M., Struiksma, N. & Van Mierlo, M. C. L. M. 1995 Laboratory measurements of the direction of sediment transport on transverse alluvial-bed slopes. *J. Hydraul. Res.* **33**, 519–534.

Tubino, M. & Seminara, G. 1990 Free-forced interactions in developing meanders and suppression of free bars. *J. Fluid Mech.* **214**, 131–159.

Yang, C. L. & Shimizu, Y. 2005 Numerical simulation of relatively wide, shallow channels with erodible banks. *J. Hydraul. Engng* **131** (7), 565–575.

Zolezzi, G., Luchi, R. & Tubino, M. 2009*a* Coupling the dynamics of channel width and curvature in meandering rivers: a perspective on fluvial patterns. In *Proceedings of RCEM 2009 Conference*, Santa Fe, Argentina, 21–25 September. Taylor & Francis.

Zolezzi, G., Luchi, R. & Tubino, M. 2009*b* Morphodynamic regime of gravel bed, single-thread meandering rivers. *J. Geophys. Res.—Earth Surf.* **114**, f01005, doi:10.1029/2007JF000968.

Zolezzi, G. & Seminara, G. 2001 Downstream and upstream influence in river meandering. Part 1. General theory and application of overdeepening. *J. Fluid Mech.* **438**, 183–211.

https://doi.org/10.1017/jfm.2011.200 Published online by Cambridge University Press